CEAS Space Journal (2019) 11:485–496
https://doi.org/10.1007/s12567-019-00277-5

ORIGINAL PAPER

Radiometric calibration of the SIMBIO-SYS STereo imaging Channel

A. Slemer[1] · V. Da Deppo[1,2] · E. Simioni[2] · C. Re[2] · M. Dami[3] · D. Borrelli[3] · I. Ficai Veltroni[3] · G. Aroldi[3] · L. Tommasi[3] · M. T. Capria[4] · G. Naletto[5,6] · R. Mugnuolo[7] · M. Amoroso[7] · G. Cremonese[2]

Received: 15 April 2019 / Revised: 1 August 2019 / Accepted: 5 September 2019 / Published online: 13 September 2019

Abstract
The STereo imaging Channel (STC) is a double wide-angle camera developed to be one of the channels of the SIMBIO-SYS instrument onboard of the ESA BepiColombo mission to Mercury. STC main goal is to map in 3D the whole Mercury surface. The geometric and radiometric responses of the STC Proto Flight model have been characterized on-ground during the calibration campaign. The derived responses will be used to calibrate the STC images that will be acquired in flight. The aim is to determine the functions linking the detected signal in digital number to the radiance of the target surface in physical units. The result of the radiometric calibration consists in the determination of well-defined quantities: (1) the dark current as a function of the integration time and of the detector temperature, settled and controlled to be stable at 268 K; (2) the read out noise, which is associated with the noise signal of the read-out electronic; and (3) the fixed pattern noise, which is generated by the different response of each pixel. Once these quantities are known, the photon response and the photo-response non-uniformity, which represents the variation of the photon responsivity of a pixel in an array, can be derived. The final result of the radiometric calibration is the relation between the radiance of an accurately known and uniform source, and the digital numbers measured by the detector.

Keywords BepiColombo · STereo imaging Channel · Radiometric calibration · CMOS detector

1 Introduction

To reconstruct the geological history of Mercury, a detailed analysis of the planet surface is needed. It includes the crustal differentiation and resurfacing, the volcanism, the tectonics and the surface/atmosphere interaction. To investigate these topics, good spatial resolution data are needed. A crucial role in the analysis of geological and mineralogical features of Mercury surface will be provided by the Spectrometer and Imagers for MPO BepiColombo-Integrated Observatory SYStem (SIMBIO-SYS) instrument suite [1].

SIMBIO-SYS includes two imaging systems with stereo and high spatial resolution capabilities, which are the STereo imaging Channel (STC) and the High Resolution Imaging Channel (HRIC), and a hyperspectral imager in the V-NIR range, named Visible and near Infrared Hyperspectral Imager (VIHI). STC performs 58–120 m spatial resolution global mapping in stereo mode and coloured imaging of selected areas; HRIC is a camera for high resolution imaging (6–12 m/px) in panchromatic and broad-band (BB) filters; VIHI performs imaging spectroscopy in the 400–2000 nm spectral range. A highly integrated concept is adopted to maximize the scientific return and minimize the resource requirements, primarily mass and power.

The main scientific goal of SIMBIO-SYS is to map the Mercury surface in different wavelengths and with different spatial resolutions to investigate the morphology and chemical composition of the planet surface. To guarantee the high quality of images acquired, it is necessary to know what fraction of the Digital Number (DN) measured by the

✉ A. Slemer
alessandra.slemer@pd.ifn.cnr.it

1 CNR-IFN Padova, Via Trasea 7, 35131 Padua, Italy

2 INAF-OAPD, Vicolo dell'Osservatorio 5, 35122 Padua, Italy

3 Leonardo S.p.A., Via delle Officine Galileo 1, Campi di Bisenzio, 50013 Florence, Italy

4 INAF-IAPS, Via del Fosso del Cavaliere 100, 00133 Rome, Italy

5 Department of Physics and Astronomy, University of Padova, Via Marzolo 8, 35131 Padua, Italy

6 CNR-IFN, Via Trasea 7, 35131 Padua, Italy

7 ASI, Via del Politecnico, 00133 Rome, Italy

detector corresponds to the real input flux. Therefore, the radiometric calibration of the detector has to be performed, which consists in the analysis of detector noises and the determination of the relation between input radiance in physical units and the DN measured. In this work a peculiar noise analysis has been performed to mitigate the residual off-set that remains after dark current subtraction. This analysis, which is due to a detector peculiarity, represents an improvement in the noise analysis and characterization with respect to previous works (e.g., [2, 3]).

This paper is structured as follows. In Sect. 2, a brief description of the STC optical concepts is reported; Sect. 3 is dedicated to the description of the on-ground calibration setup and to the definition of the radiometric calibration pipeline; Sect. 4 reports the preliminary results and some corollary considerations. Finally, Sects. 5 and 6 show in detail the calibration process applied to a test image.

2 The STereo imaging Channel

The STC channel is a stereo-camera that consists in two sub-channels which deflect the light, coming from two different directions, on one common detector [4] (see Fig. 1). The two STC sub-channels are named H (High) and L (Low) following their position with respect to the mounting interface on the S/C. For each sub-channel, STC can acquire simultaneously three quasi-contiguous areas of the Mercury surface in different colors, one panchromatic and

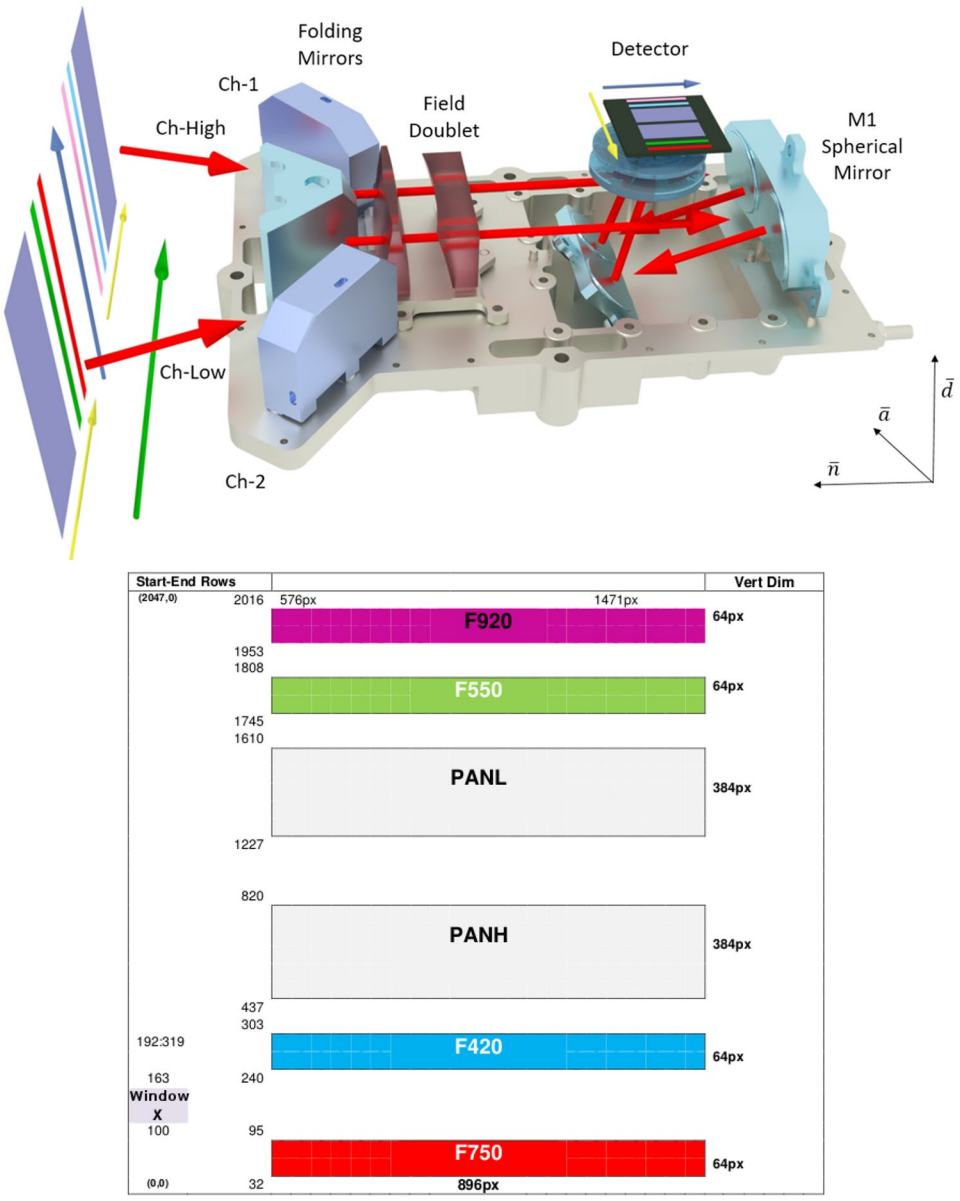

Fig. 1 STC optical scheme and detector configuration

two BB [5]. The central ray of the panchromatic filter of each sub-channel forms an angle of ± 21.375° with respect to the nadir direction.

The characteristics of the STC optical design and the scientific requirements are summarized in Table 1. STC is different from conventional on-axis reflecting and catadioptric telescopes, such as Schmidt and Maksutov. Adopting an off-axis layout, central obstruction, spiders, or other support structures, are not necessary. This solution guarantees to obtain better optical performance in terms of Point Spread Function (PSF) and Modulation Transfer Function (MTF) compared to the on-axis obstructed systems.

The pair of folding mirrors, located at the entrance of each optical sub-channel, guides the incoming light to a common Schmidt modified telescope. The telescope has a focal length of 95.2 mm. The camera is equipped with four broad-band (BB), or color, filters, each one having 20 nm bandwidth (centered at 420 nm, 750 nm, 550 nm and 920 nm), and two panchromatic (PAN) filters, whose bandwidth is 200 nm, centered at 700 nm. The filters are mounted on the detector following the configuration shown in Fig. 1.

The nominal FoV of each sub-channel is 5.38° × 4.8°, which includes gaps, while the scientific useful FoV is 5.38° × 3.07°. The latter FoV is divided in three portions that correspond to the filters of the considered sub-channel: 5.38° × 2.31°, for the PAN filter, and 5.38° × 0.38°, for each color filter. STC will perform 58–120 m spatial resolution global mapping in stereo mode and coloured images of selected areas in color mode. The STC detector is a 2048 × 2048 hybrid Si-PIN detector, with a backside illuminated Si-PIN sensitive area coupled to a CMOS readout integrated circuit; it has 10 µm of pixel size and a dynamic range of 14 bit. The Integrate Then Read (ITR) technology allows to avoid a mechanical shutter. The choice of this detector has been driven by three main reasons: (1) to acquire images with very short integration time (IT); (2) to reach the fill-factor of 100%; and (3) to avoid the detector degradation due to radiations. Using this detector, it is easy to obtain millisecond exposure times that are needed to reduce the possible image smearing, due to the motion of the S/C with respect to the Mercury surface.

3 On ground radiometric calibration pipeline

The geometric and radiometric responses of the STC Proto Flight Model (PFM) have been characterized on-ground in during the calibration campaigns [7, 8]. The derived responses will be used as starting point for the calculation of the calibration key data parameters that will be refined with the in-flight calibration.

The calibration pipeline, developed to convert the raw data images into images whose pixel value is expressed in physical units, includes the dark current removal, radiometric conversion and geometric distortion correction.

In this section we briefly describe the experimental setup used for the instrument calibration and the procedure developed to derive the calibrated images.

3.1 Calibration setup

The Optical Ground Support Equipment (OGSE) used for the STC calibration was developed by Leonardo S.p.A. and located in a cleanroom. The OGSE experimental setup is shown in Fig. 2. It is composed of: (1) different optical elements mounted on the Optical Bench (OB) used to provide the optical stimulus; (2) the Thermal Vacuum Chamber (TVC), where the STC PFM is mounted; and (3) the TVC control system (see left panel of Fig. 2). The incoming light beam passes through an optical window on the TVC before reaching each of the STC sub-channels [9].

During the on-ground calibration, the detector dark current temperature dependence has been measured. The TVC guarantees the control of the temperature of the mechanical structure, while an active Thermo Electric Cooler (TEC), which is included in the Focal Plane Assembly (FPA), controls the temperature of the Focal Plane Assembly (FPA) [9].

Table 1 Optical characteristics and scientific requirements of STC [6]

Optical characteristics	
Optical concept	Catadioptric: off-axis portion of a modified Schmidt telescope with folding mirror fore-optics
Stereo solution	Two optical channels with detector and most of the optical elements in common
Focal length	95.2 mm
Pupil size	15 mm (diameter)
IFOV	105 µrad/px
Focal ratio	6.3
Distortion	< 0.3%
FoV (cross track)	5.38°
FoV (along track)	2.4° for panchromatic, 0.38° for color filters

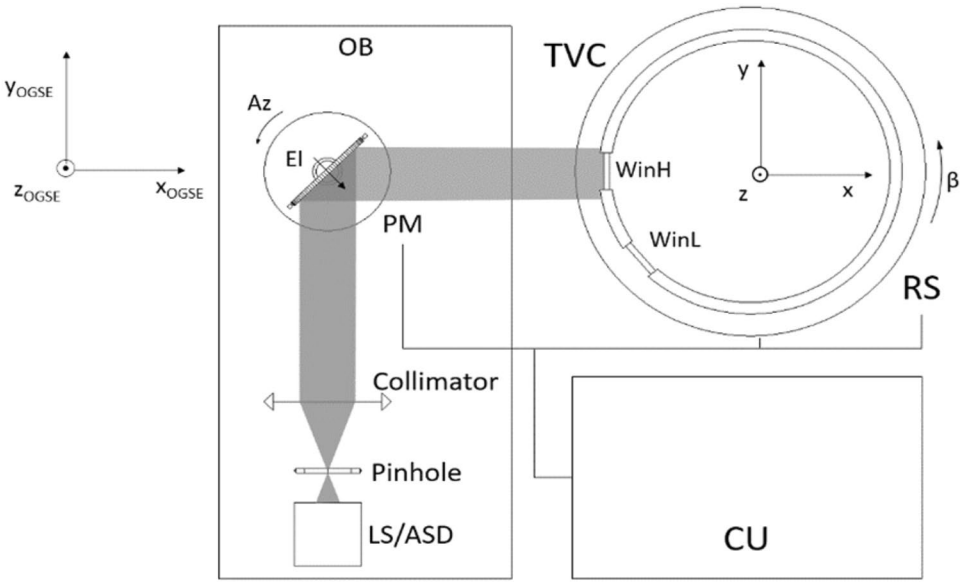

Fig. 2 Schematic representation of the OGSE [6]. The light flux that exits from the Light Source (LS), pass throughout a pinhole and then is collimated by the collimator. A Plane Mirror (PM) deflects the collimated light beam towards the Thermal Vacuum Chamber (TVC), which is mounted on a Rotational Stage (RS). The RS can rotate around the vertical direction and the rotational angle is β. To enter the TVC, and to reach the STC instrument which is mounted inside, the light passes through a window (WinH/WinL). The PM and RS orientations are controlled by the Control Unit (CU)

The radiometric calibration has been performed to derive the instrument response and characterize the spatial and temporal noise.

3.1.1 Integrating sphere characterization

For the radiometric calibration, to fully cover the expected radiance range, an Integrating Sphere (IS) with variable flux has been used [9]. The IS used for the STC calibration is a Labsphere ISS-2000-C, provided with four halogen lamps, one of which is equipped with a shutter. Each lamp can be powered on and off independently. The technical characteristics of the integrating sphere are shown in Table 2.

3.2 Calibration pipeline

This section describes the pipeline used to obtain the radiometric calibration relations for each pixel. The steps of the procedure have been sketched in Fig. 3. The data reduction process for one acquisition session is fully described.

The acquired data are organized in six different sessions, each one containing the images in which a specific filter has been illuminated. The images within different sessions have been acquired with an ad-hoc set of ITs to cover the range in which the detector response is expected to be linear. The IT sets are different for each filter given the different filter sensitivity. Two sets of images have been acquired for the same ITs values: either in dark condition, or illuminated by the IS.

The calibration procedure starts with the reading of the raw files. To mitigate the noise effects, in each session ten images with the same IT have been acquired and averaged for each pixel of the frame. Also the standard deviation (std) has been calculated for each pixel. This step of the pipeline has been called Read Out Noise (RON) reduction.

Then, the dark current contribution has to be subtracted. Since the dark current depends on the ITs, and the DC calibration has not been performed at all the possible ITs,

Table 2 Technical characteristics of the integrating sphere

IS specifications	
Inner diameter	20″ (50 cm)
Aperture diameter	8″ (20 cm)
Inner wall coating and reflectance	Spectraflect®/98%
Lamp configuration (number and rated power)	Three 35 W lamps, one 100 W lamp
Lamp type	Tungsten halogen
Color temperature	3000 K
Lamp power supply current stability (35 W/100 W)	3.07 A ± 0.1%/8.33 A ± 0.1%
Peak radiance (at 900 nm)	550 $W/m^2/sr/\mu m$
Luminance uniformity (at maximum radiance level)	98%
Internal monitor detector	Silicon detector

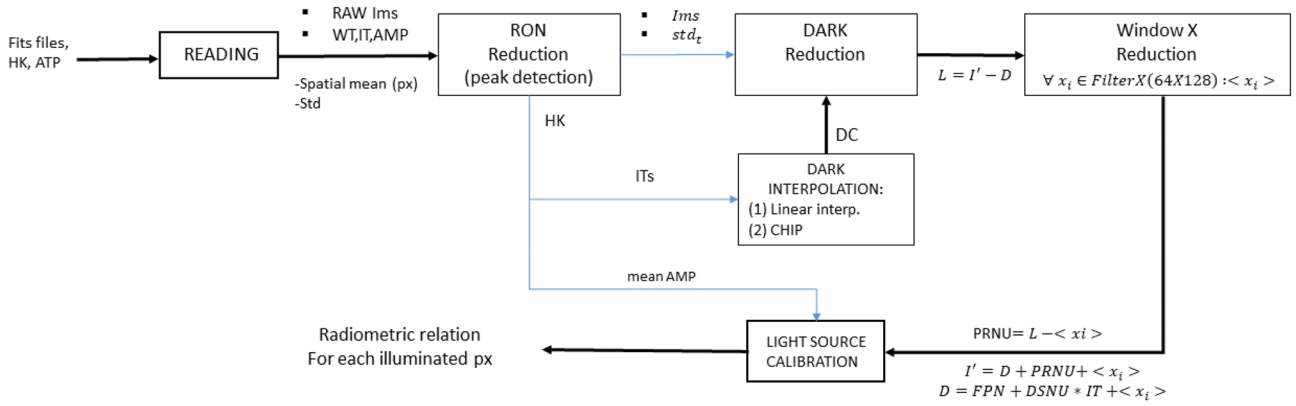

Fig. 3 Flow chart of the radiometric calibration pipeline

the DC values for the considered IT have to be derived via interpolation. The interpolation can been performed in two ways: with a linear interpolation or using the Cubic Hermite Interpolation Polynomia (CHIP).

Furthermore, the off-set mitigation has to be performed to remove a remaining off-set residual due to an anomalous behavior of the STC CMOS detector [10]. The method adopted for the off-set mitigation is a definition of an additive window on the detector, which is called Window X (see Fig. 1). This additive windows sits in a dark coated region of the detector, so that the signal measured by WIndows X is not due to light photons.

Finally, the relation between the integrating sphere flux (in physical units) and the values in DN detected can be calculated.

Here follows the detailed description of each calibration step.

3.2.1 RON reduction

The Read Out Noise (RON) comes from the CMOS readout circuit that is responsible for the conversion of the charge collected in each pixel into a voltage that is converted in Digital Number (DN). To reduce the impact of the spatial noise and of the RON, for each session ten images with the same IT have been acquired and then averaged.

In the upper panel of Fig. 4, the mean of a group of ten images is depicted. The image includes the entire H-channel and it refers to the session of PANH filter with IT = 0.83 ms (which corresponds to an IT in the linearity range of the detector response curve). The bottom panel shows the image of the standard deviations calculated for each pixel from the same ten images used for the upper image. The standard deviation in the non-illuminated regions gives an estimate of the Read Out Noise (RON), since the integration time is relatively small, while the std in the illuminated region includes also the effect of the photon noise.

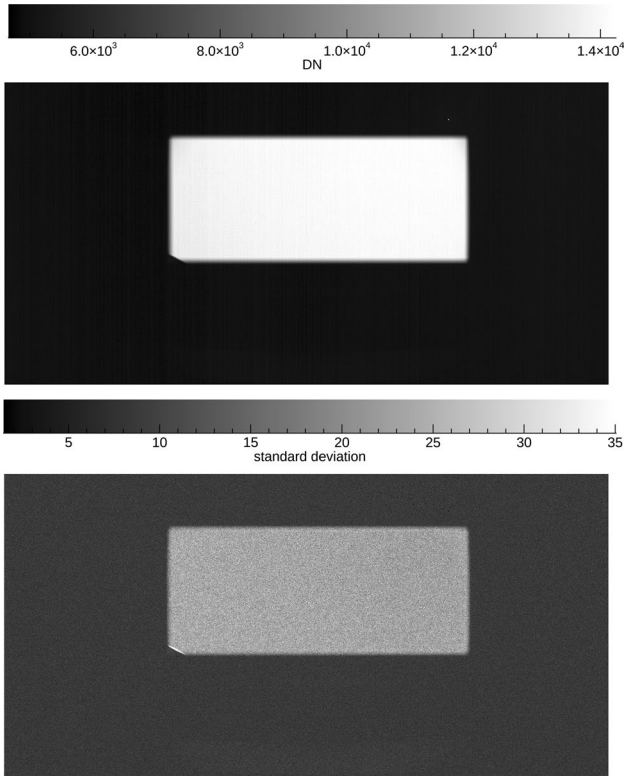

Fig. 4 Top panel: mean image (averaged over 10 images) of the sub-channel H at IT = 0.83 ms. Bottom panel: standard deviation in DN. Both images are relative to the acquisition session of the PANH filter. Despite the image represents the entire sub-channel H, the two color filters (420 nm and 750 nm) are not visible for two different reasons: (1) the QE of the detector at 420 nm is lower with respect those at higher wavelength; (2) the bandwidth of BB filters is 1/10 of those of PAN filters, so that neither the 750 nm filter can be seen

3.2.2 Dark current subtraction

The behavior of the dark current (DC) as a function of the IT and detector temperature has to be known. The nominal

operating temperature of the detector is 268 K [10]. Figure 5 shows the mean detector DC curve as function of IT for the temperature interval between 263 and 273 K. The DC of the STC channel detector is characterized by two different trends. For ITs lower than 1 ms the DC increasing is almost exponential, while for ITs longer than 1 s (foreseen for stellar acquisitions) it is linear.

To subtract the dark current contribute, the values of dark current relative to each pixel of the detector have to be interpolated at the ITs correspondent to those of the calibration session considered. The interpolation functions used to obtain the correct dark current are the linear function and the Hermitian spline.

3.2.3 Background subtraction

The dataset acquired for the radiometric calibration includes also the background images. These images are acquired with the light source covered to estimate the background detected signal. For each acquisition session, the background images have been acquired at the same ITs used to image the light source.

Figure 6 shows the image of PANH after the background removal at IT = 0.83 ms, which corresponds to an IT in the detector linearity range. The image corresponds to a mean of ten raw images taken at the same IT. Figure 7 shows the central column profile for two different ITs, 0.14 ms (red line) and 0.83 ms (blue line). Both the profiles show that in the dark regions of the detector the DN value is not equal to zero.

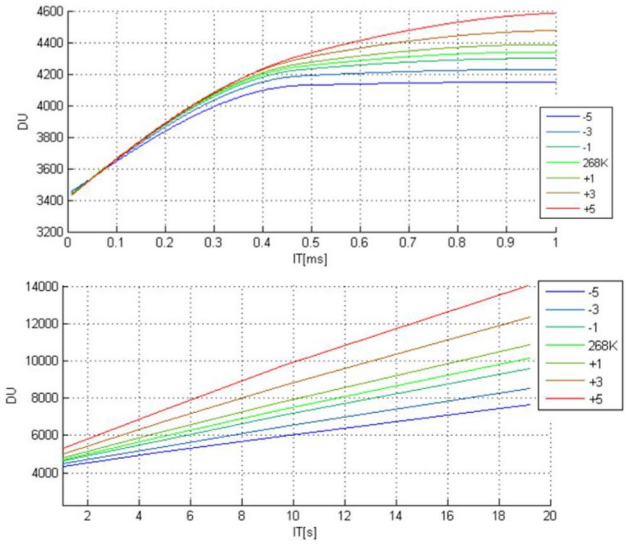

Fig. 5 Mean detector dark current as function of IT and measured in the range 263–273 K with temperature intervals of 2 K. Top panel shows the DC for ITs from 400 ns to 0.96 ms, while the bottom panel from 9.6 ms to 19.6 s

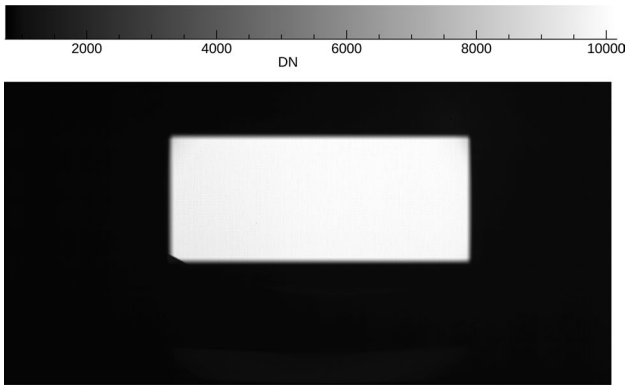

Fig. 6 Image of PANH session after background removal, at IT = 0.83 ms

This non-expected behaviour of the detector, which depends by the IT and the Repetition Time (RT), can be mitigated by measuring the value of a non-illuminated region of the detector, which has been called window-X. The window-X has dimension 64 × 128 pixels. For more details see Refs. [10] and [7]. The result of the background and window-X reduction is the Photo Response (PR) of the detector, which has been derived for each filter separately.

3.2.4 Dark signal non uniformity

The CMOS detector is also characterized by a Dark Signal Non Uniformity (DSNU), which is the noise generated by the different response of each pixel in absence of illumination for a low integration time, nominally 0. To characterize the DSNU of the CMOS, a series of images has been acquired at low IT (few millisecond) and in dark condition at nominal temperature of 268 K [10].

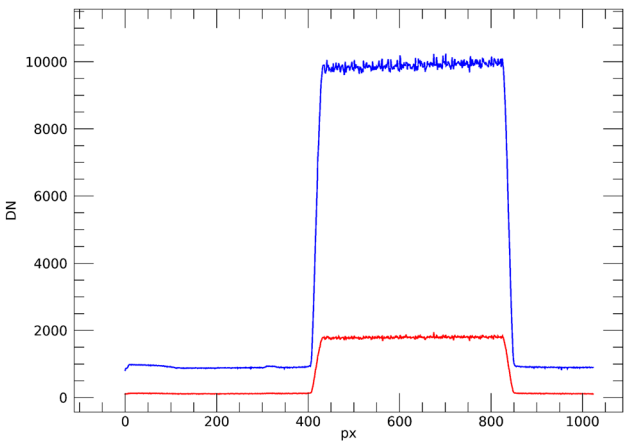

Fig. 7 Line profile of PANH session image after background removal, for the central column of the detector. The blue line refers to IT = 0.83 ms (it represents the raw profile of Fig. 6), while the red line refers to the IT = 0.14 ms

The standard deviation of the DSNU is 135 DN RMS for the dark images acquired with IT < 10 ms, independently from the temperature. For higher IT the standard deviation of the DSNU reaches 400 DN RMS (on a dynamic of 14 bits) [7].

3.2.5 Photon response

Once DC and FPN are known, the Photo Response (PR) and the Photo Response Non-Uniformity (PRNU) can be derived. For an imaging detector, the PR measures the ability to convert optical incident power (i.e., the number of impinging photons for a given exposure time) into an electrical signal. The PRNU represents the RMS variation of the photo-responsivity of the pixels in the array under the same illumination condition [11].

Figure 8 shows the row profile along the central column of the PANH filter in PANH session, at IT = 0.83 ms. As expected, the signal in dark regions is equal to zero. The non-uniformity of the signal for different lines represents the PRNU of the detector. The slight signal present at rows 5–100 is the signal detected in the region correspondent to the 750 nm filter, as well as the faint signal present at rows 300–340 due to 420 nm filter.

To obtain the radiometric calibration it is necessary to find the relation between the photo response of the detector and the amount of light incoming to the optical system. Therefore, also the light source has to be characterized and calibrated.

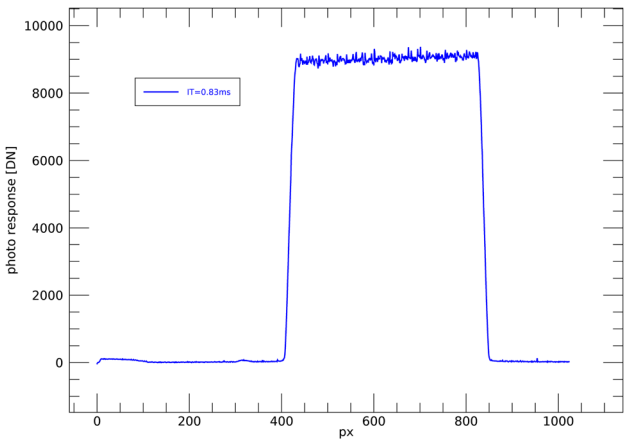

Fig. 8 line profile of the photo response of the PANH session image, at IT = 0.83 ms

4 Preliminary results

The final result of the radiometric calibration consists in the determination of the relation between the signal expressed in DN and the signal expressed in physical units. Namely, the absolute radiometric calibration is the relation between the detected signal and the radiance value of an accurately known source illuminating the instrument.

This relation has been derived for each pixel of the illuminated region of the detector, to obtain a map that will be used to calibrate the raw images. Figure 9 shows the mean values of the slopes of the radiometric function. The photo response has been obtained by subtracting the background images, and the results refers to the detector linearity range and are obtained for each filter of the detector.

These results represent a starting point for some interesting considerations. First of all, by looking at the PAN filters, the values of the slopes in the right hand side of the detector are lower than those in the left side. This behavior can be due to different causes: the CMOS detector response may be affected by the imperfections of its sensitive surface; another cause of the left–right different slopes can be due to the spurious effects such as straylight inside the TVC.

This effect is confirmed by Fig. 10, which represents the statistics of the slope distribution shown for each filter separately. The histograms relative to PANH and PANL show a double-Gaussian profile, which is related to the left–right different behavior shown in Fig. 9. The plots relative to BB filters show that the left–right difference in sensitivity is slightly observed. The more accentuated spread for the 420 nm filter can be explained by considering that for the light at 420 nm the absorption depth in silicon is lower than those for the light at higher wavelength. The non-uniformity of the detector response (Fig. 9) is more evident at 420 nm, because the photon interaction occurs in a region, where there are imperfections. the at higher wavelength.

These considerations, together with the fact that the panchromatic optical path has no particular characteristics which could introduce a flat fielding effect, confirms the hypothesis that this cross track trend should be due to the calibration setup.

Since the DN value varies with the amount of light flux, it is interesting to show the DN-flux dependence. Figure 11 shows the relation between light flux and DN of the central pixel with varying the DN value detected, for each filter. The results refers to the images after the background and off-set reduction, so that the DN interval has been chosen from 0 to 8000 DN. As expected, the relations are linear for all the filter considered. The change of the slopes can be viewed for high DN values of 420 filter and it corresponds to the values near the detector saturation.

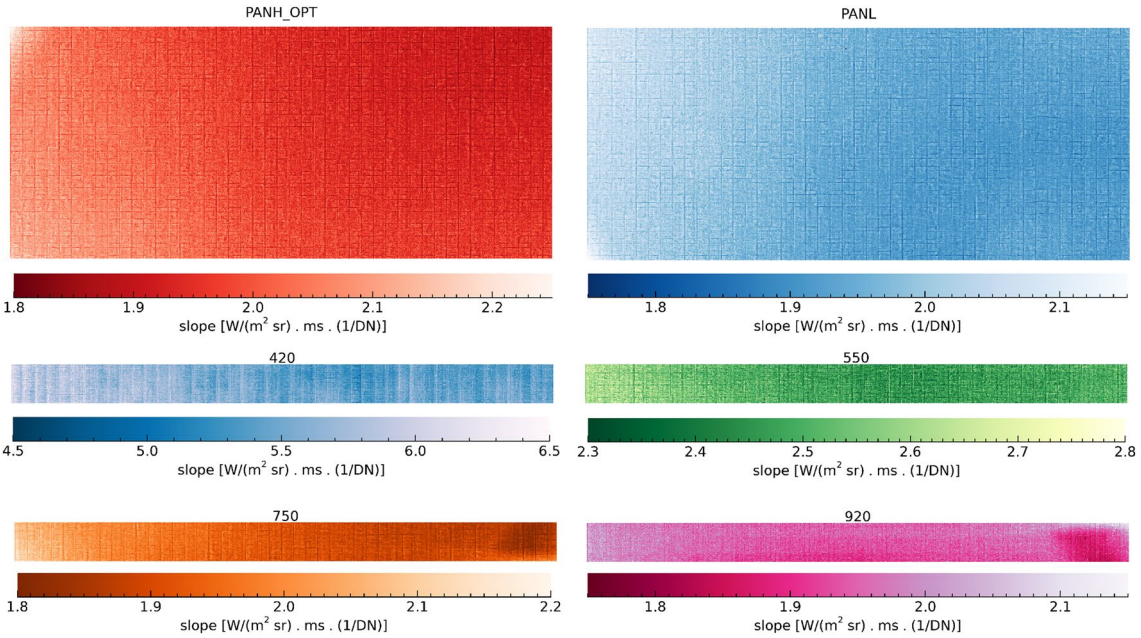

Fig. 9 Mean values of radiometric function in the linearity range, for each filter of the STC detector. The photo response has been obtained using the background images

5 Statistical errors

The procedure used to obtain the error that affects the calibration curve starts form the equation:

$$y = \frac{\partial f}{\partial x} \cdot x, \tag{1}$$

where y represents the integrated flux in the filter bandwidth in physical units ($W/m^2/sr$) and x is the DN values revealed by the detector. Taking into account the error that affects the input flux and the DN values detected, Eq. 1 becomes

$$y + \Delta y = \left(\frac{\partial f}{\partial x} \pm \delta \right) \cdot (x \pm \Delta x), \tag{2}$$

where δ represents the error that affect the calibration curve, and Δx is the error that affect the photon detection. Since the calibration curve is the ratio between the input flux in physical unit and the DN values detected by the CMOS sensor, the value of δ_{rel} is the sum of the relative errors that affect both quantities:

$$\delta_{\text{rel}} = \epsilon_{\text{IS}} + \epsilon_{\text{QE}} + \epsilon_{\text{filter}} + \epsilon_{\text{T}}. \tag{3}$$

The terms represent, respectively, the errors of the flux of the integrating sphere, the detector quantum efficiency, the filter transmittance and the optic transmittance. The absolute value of δ is $\delta_{\text{rel}} \cdot \partial f / \partial x$.

The error Δx is determined by the quantities that affect the photon detection. In this work only the QE, the efficiency of the filter and the optic transmittance has been considered. So that

$$\Delta x = x \cdot (\epsilon_{\text{QE}} + \epsilon_{\text{filter}} + \epsilon_{\text{T}}). \tag{4}$$

The results has been represented in the histograms of Fig. 12. Each plot shows the error related to the slope of the calibration relation in the linearity range. From the plot it results that the error spans from 23 to 28%.

The calibration curve is affected also by the errors generated by the calibration procedure: the dark interpolation, the background and off-set subtraction. To give the preliminary results, this work does not consider the scenario obtained with the dark subtraction, so that the error generated by the dark interpolation has not been considered. The latter analysis will be taken into account after the data reduction of the in-flight dark campaign, which is acquired during the Near Earth Commissioning Phase (NECP) [12]. The total error generated by the sum of these contributes without taking into account the dark interpolation error is around 1–2%, so that it represents a small contribution with respect to the total relative error calculated.

6 Calibration of sample images

To verify the reliability of the calibration relation, a set of test images has been acquired with the STC and then calibrated. Figure 13 shows a test image after the background and off-set reduction (top panel) and after the radiometric

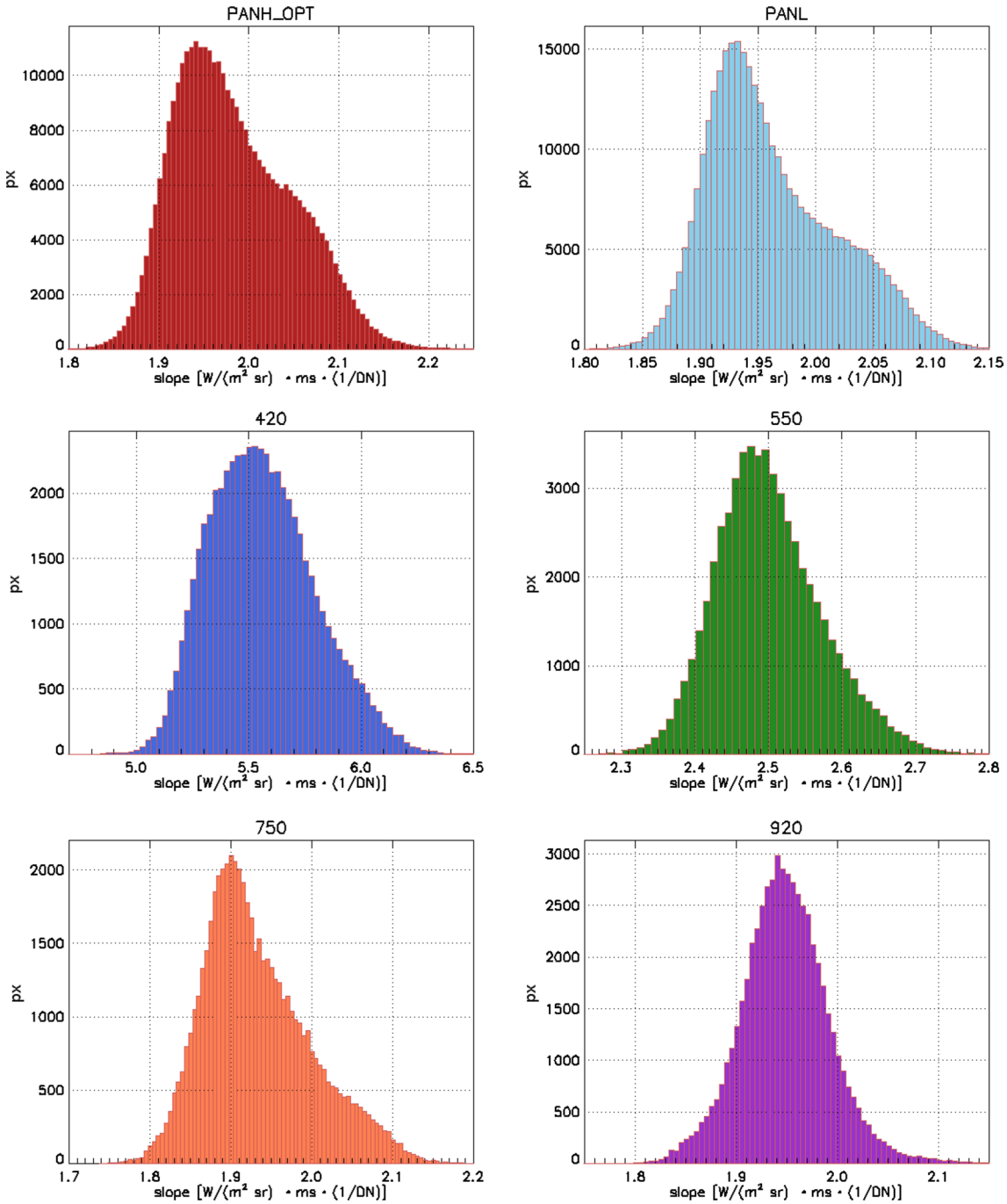

Fig. 10 Statistics of the slope of the radiometric curve of Fig. 9, for the PAN and BB filters of STC detector

calibration (bottom panel) [13]. The image has been acquired with the filter PANH, with IT = 1.92 ms. The top image represents the signal detected in DN, while the bottom image shows the signal in $W/m^2/sr\,ms$, which consists in the product between the flux integrated in the bandwidth of the filter considered and the IT. The "weft-effect" visible in the top image is the PRNU. After the radiometric calibration, this effect disappears, so that the final image represents the actual flux coming from the object observed and detected by the CMOS detector.

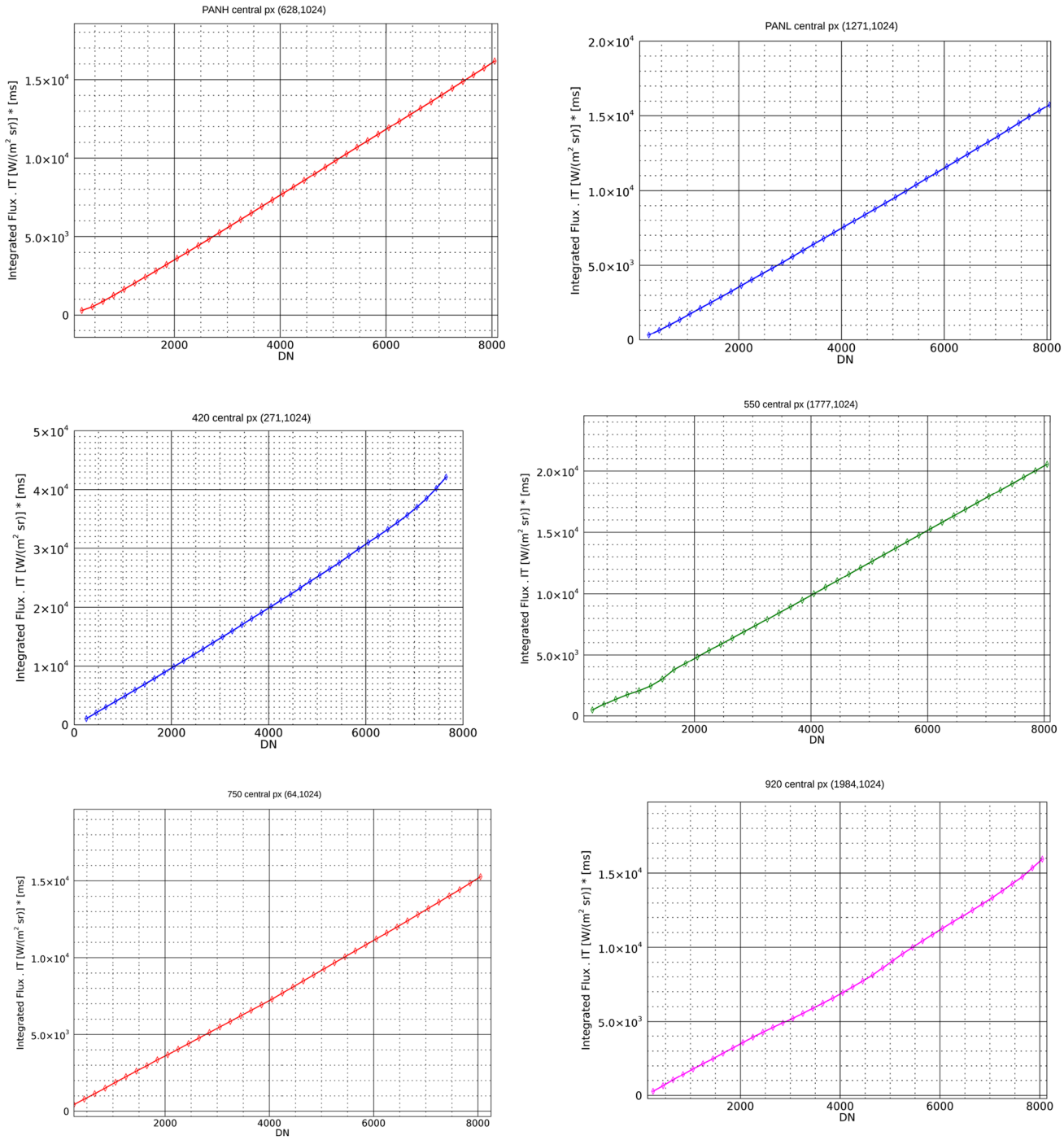

Fig. 11 Radiometric calibration curves for the central px of each filter. The *y*-axis represents the flux integrated in the filter-bandwidth multiplied for the IT, while the *x*-axis shows the DN detected

7 Conclusions

This work shows the radiometric calibration function of the STC CMOS detector, describing the method used to derive it. The calibration function has been obtained for each pixel of the illuminated regions of the detector, because the photoresponse varies with the region of the CMOS detector considered. The results consist in the mean slope of the calibration function, which refers to the linearity range of the response curve of the detector. The left–right disparity in the slope of the radiometric function obtained for PAN filter and the different between the mean slope of BB filters can

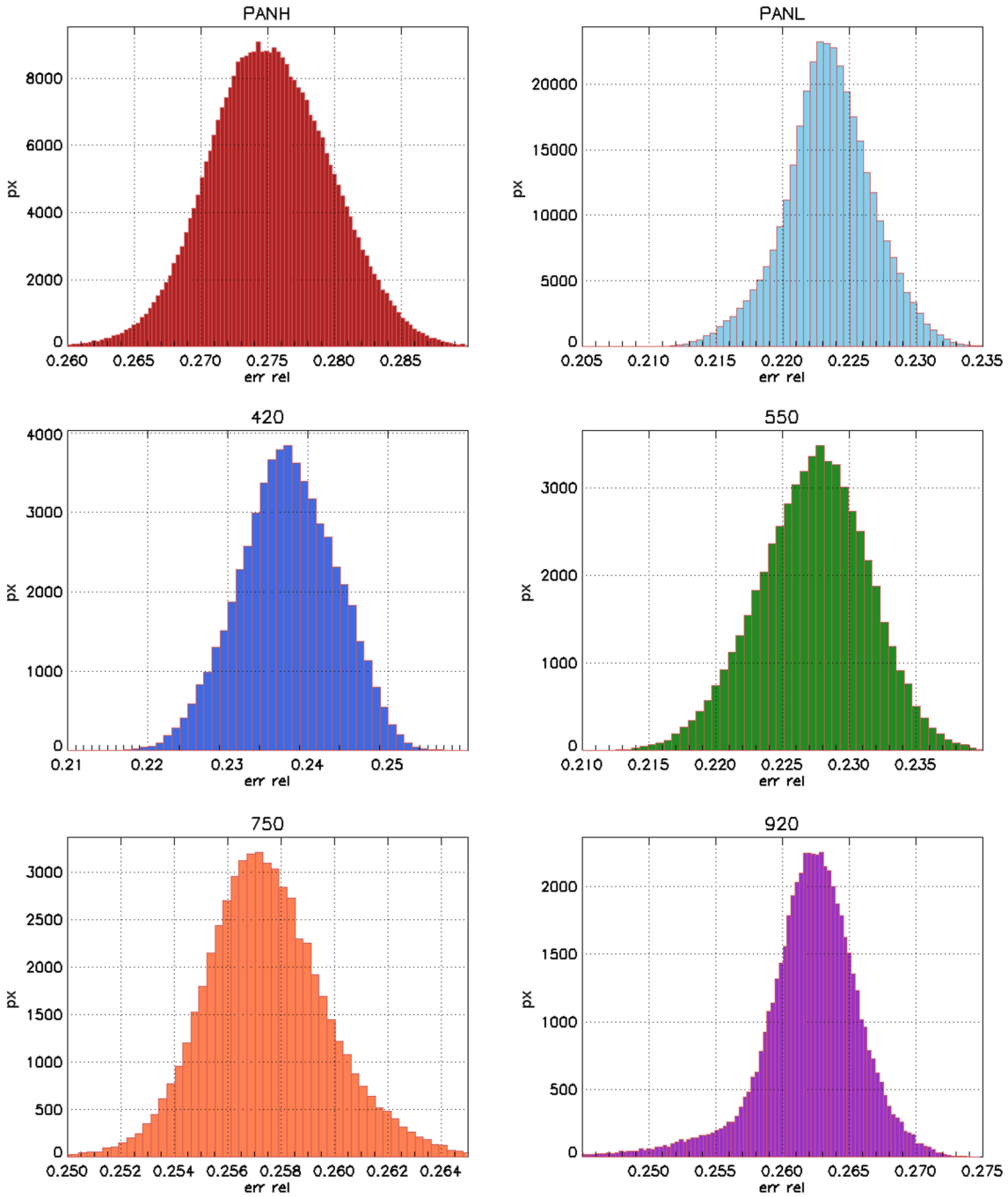

Fig. 12 Histograms of the relative error associated to the value of radiometric function in the linearity range, for each filter of the STC detector

be explained by considering the different absorption depths of photons with different wavelengths in silicon. The results here obtained can be applied to calibrate images for which DN values measured by the detector are far from the saturation level.

The calibration curves can be used to test the values of the filter and optics transmittance. The test consists in a comparison between the actual input flux relative to specific DN values and the expected DN/ms for a specific input flux in physical units. The expected flux in DN/ms can be estimated with the radiometric model for SIMBIO-SYS instrument [14]. A future work can be devoted to this analysis.

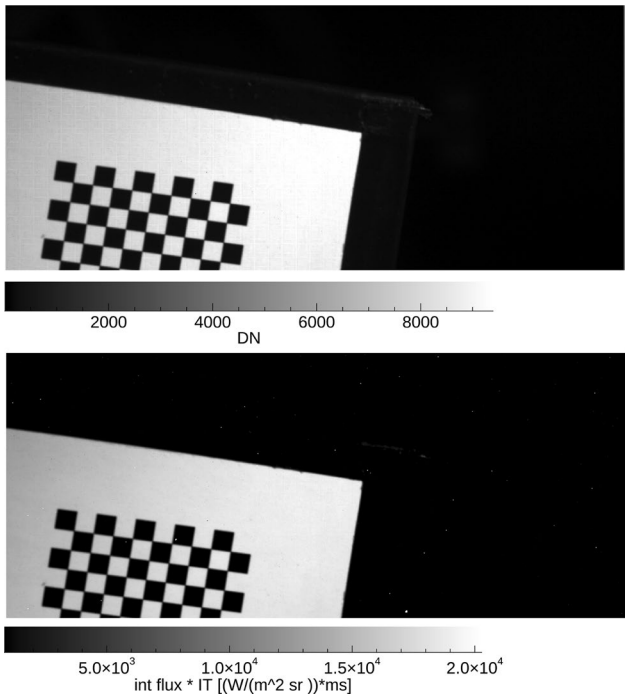

Fig. 13 Test image before the background and offset reduction (top panel) and after the radiometric calibration (bottom panel). The images has been acquired with filter PANH

Acknowledgements We gratefully acknowledge funding from the Italian Space Agency (ASI) under ASI-INAF agreement 2017-47-H.0. The SIMBIO-SYS instrument has been developed by Leonardo under ASI contract I054/10/0.

References

1. Flamini, E., Capaccioni, F., Colangeli, L., Cremonese, G., Doressoundiram, A., Josset, J.L., Langevin, Y., Debei, S., Capria, M.T., de Sanctis, M.C., Marinangeli, L., Massironi, M., Mazzotta Epifani, E., Naletto, G., Palumbo, P., Eng, P., Roig, J.F., Caporali, A., Da Deppo, V., Erard, S., Federico, C., Forni, O., Sgavetti, M., Filacchione, G., Giacomini, L., Marra, G., Martellato, E., Zusi, M., Cosi, M., Bettanini, C., Calamai, L., Zaccariotto, M., Tommasi, L., Dami, M., Ficai Veltroni, J., Poulet, F., Hello, Y., Simbio-Sys Team: SIMBIO-SYS: the spectrometer and imagers integrated observatory system for the BepiColombo planetary orbiter. Planet. Space Sci. **58**, 125–143 (2010)
2. Chi, Z., Suying, Y., Jiangtao, X.: Noise in a cmos digital pixel sensor. J. Semicond. **32**(11), 115005 (2011)
3. Brouk, I., Nemirovsky, A., Nemirovsky, Y.: Analysis of noise in CMOS image sensor. In: 2008 IEEE International Conference on Microwaves, Communications, Antennas and Electronic Systems, pp. 1–8. IEEE (2008)
4. Cremonese, G., Fantinel, D., Giro, E., Capria, M .T., Da Deppo, V., Naletto, G., Forlani, G., Massironi, M., Giacomini, L., Sgavetti, M., Simioni, E., Debei, S., Bettanini, C., Zaccariotto, M., Patrizia Borin, P., Marinangeli, L., Calamai, L., Flamini, E.: The stereo camera on the bepicolombo ESA/JAXA mission: a novel approach. Adv. Geosci. Planet. Sci. (PS) **15**, 305–322 (2009)
5. Da Deppo, V., Naletto, G., Cremonese, G., Calamai, L.: Optical design of the single-detector planetary stereo camera for the BepiColombo European Space Agency mission to Mercury. Appl. Opt. **49**, 2910 (2010)
6. Da Deppo, V., Martellato, E., Simioni, E., Naletto, G., Cremonese, G.: Radiometric model for the stereo camera STC onboard the BepiColombo ESA mission. In: Modeling, Systems Engineering, and Project Management for Astronomy VI. SPIE Proc., vol. 9911, 99111T (2016)
7. Simioni, E., Da Deppo, V., Re, C., Slemer, A., Capria, M. T., Veltroni, I. F., Dami, M., Borrelli, D., Tommasi, L., Cremonese, G.: The pre-launch distortion definition of SIMBIO-SYS/STC stereo camera by rational function models. In: Space Telescopes and Instrumentation 2018: Optical, Infrared, and Millimeter Wave, Society of Photo-Optical Instrumentation Engineers (SPIE) Conference Series, vol. 10698, p. 1069850 (2018)
8. Slemer, A., Simioni, E., Deppo, V.D., Zusi, M., Re, C., Lucchetti, A., Dami, M., Borrelli, D., Veltroni, I.F., CaPria, M.T., Cremonese, G.: Performances of the simbio-sys stereo imaging channel (STC) on board bepicolombo/esa spacecraft. In: 2018 5th IEEE International Workshop on Metrology for AeroSpace (MetroAeroSpace), pp. 257–262 (2018)
9. Da Deppo, V., Martellato, E., Rossi, G., Naletto, G., Della Corte, V., Capaccioni, F., Filacchione, G., Zusi, M., Palumbo, P., Aroldi, G., Baroni, M., Borrelli, D., Tommasi, L., Dami, M., Ficai Veltroni, I., Flamini, E., Cremonese, G.: Characterization of the integrating sphere for the on-ground calibration of the SIMBIOSYS instrument for the BepiColombo ESA mission. In: Space Telescopes and Instrumentation 2014: Optical, Infrared, and Millimeter Wave, SPIE Proc., vol. 9143, p. 914344 (2014)
10. Simioni, E., De Sio, A., Da Deppo, V., Naletto, G., Cremonese, G.: CMOS detectors: lessons learned during the STC stereo channel preflight calibration. In: Society of Photo-Optical Instrumentation Engineers (SPIE) Conference Series, Society of Photo-Optical Instrumentation Engineers (SPIE) Conference Series, vol. 10562, p. 105622M (2017)
11. Hopkinson, G.R., Goodman, T.M., Prince, S.R.: A Guide to the Use and Calibration of Detector Array Equipment, vol. 142. SPIE Press, Bellingham (2004)
12. Simioni, E., Re, C., Da Deppo, V., Naletto, G., Borrelli, D., Dami, M., Ficai Veltroni, I., Cremonese, G.: Indoor Calibration for Stereoscopic Camera STC: A New Method, vol. 10563 (2017)
13. Naletto, G., Cesaro, M., Albasini, A., Cremonese, G., Da Deppo, V., Forlani, G., Re, C., Roncella, R., Salemi, G., Simioni, E.: Innovative Optical Setup for Testing a Stereo Camera for Space Applications, vol. 8442 (2012)
14. Slemer, A., Zusi, M., Simioni, E., Da Deppo, V., Re, C., Della Corte, V., Filacchione, G., Palumbo, P., Capaccioni, F., Cremonese, G.: A Mercury surface radiometric model for SIMBIO-SYS instrument suite on board of BepiColombo mission. In: Space Telescopes and Instrumentation 2018: Optical, Infrared, and Millimeter Wave, Society of Photo-Optical Instrumentation Engineers (SPIE) Conference Series, vol. 10698, p. 106984C (2018)